

Isogeometric thermal postbuckling of FG-GPLRC laminated plates

Y. Kiani ^{*1} and M. Mirzaei ^{2a}

¹ Faculty of Engineering, Shahrood University, Shahrood, Iran

² Department of Mechanical Engineering, Faculty of Engineering, University of Qom, Qom, Iran

(Received May 1, 2019, Revised September 4, 2019, Accepted September 6, 2019)

Abstract. An analysis on thermal buckling and postbuckling of composite laminated plates reinforced with a low amount of graphene platelets is performed in the current investigation. It is assumed that graphene platelets are randomly oriented and uniformly dispersed in each layer of the composite media. Elastic properties of the nanocomposite media are obtained by means of the modified Halpin-Tsai approach which takes into account the size effects of the graphene reinforcements. By means of the von Kármán type of geometrical nonlinearity, third order shear deformation theory and nonuniform rational B-spline (NURBS) based isogeometric finite element method, the governing equations for the thermal postbuckling of nanocomposite plates in rectangular shape are established. These equations are solved by means of a direct displacement control strategy. Numerical examples are given to study the effects of boundary conditions, weight fraction of graphene platelets and distribution pattern of graphene platelets. It is shown that, with introduction of a small amount of graphene platelets into the matrix of the composite media, the critical buckling temperature of the plate may be enhanced and thermal postbuckling deflection may be alleviated.

Keywords: thermal postbuckling; graphene platelets; NURBS-based isogeometric analysis; Halpin-Tsai rule; nanocomposite

1. Introduction

Graphene is two dimensional structures which was discovered in 2004 (Novoselov *et al.* 2004). It is a monolayer structure which has the thickness equal to an atom. The repeated structure of the graphene is composed of atoms which are joined together with bundles. Graphene has shown high electrical and thermal conductivities, superior mechanical strength and large specific surface area. Comparison of graphene with the other well-known nanostructure, i.e., nanotube reveals that, production of graphene requires less costs. Considering the above mentioned characteristics of the graphene have resulted into the vast investigations to explore the extraordinary features of graphene. Among them one may refer to (Reddy *et al.* 2006, Scarpa *et al.* 2009, Cadelano *et al.* 2009, Ni *et al.* 2010, Zhang *et al.* 2011). In these researches and many other available works, the potential of graphene as a promising reinforcement for the composites is highlighted.

The graphene layer, as reported in the open literature is stiffer than most of the engineering metals such as stainless steel. The elasticity modulus of this monolayer in most of the investigations is reported as 1 TPa. Graphene has shown excellent conduction capacity even more than copper and silver. Other features of graphene as reinforcement are highlighted in (Stankovich *et al.* 2006, Potts *et al.* 2011, Das and Prusty 2013). It is also shown that, introduction of

even a low amount of graphene as reinforcement in a composite media, results in better thermal, mechanical and electrical properties (Rafiee *et al.* 2009a, Zhao *et al.* 2010). Owing to its geometry, in many applications, graphene is preferred to carbon nanotube due to the higher interaction of the graphene with matrix in comparison to carbon nanotube (CNT) with matrix.

In many experimental investigations, it is also verified that stability response of an elastic media may be enhanced significantly when graphene is inserted into the matrix with even low weight fraction. For instance, Rafiee *et al.* (2009b) conducted experiments to examine the enhancement of the buckling capacity of epoxy beams which are reinforced with graphene. As reported in this research, with introduction of low weight fraction of graphene in the matrix, the buckling loads of the composite beams may be enhanced. For instance, when only 0.1 percent of graphene is inserted into the matrix, the buckling load of the composite beams may be increased about 50%. In another investigation, Parashar and Mertiny (2012) conducted a set of simulations to analyse the buckling of graphene-epoxy composite plates under the action of unidirectional compression. Conclusion of this study is the same with the one reported by Rafiee *et al.* (2009b). For instance 26% increase in the buckling load of the plate may be achieved when the matrix of the composite media is enriched with only 6% percent of the graphene.

It should be highlighted that, the volume(weight) fraction of graphene as filler cannot be increased arbitrarily since higher volume fraction of graphene as reinforcement results in unpleasant results (Kulkarni *et al.* 2010).

Graphene as reinforcement is observed in two shapes; i.e., graphene sheets and graphene platelets. Both of these

*Corresponding author, Ph.D.,

E-mail: y.kiani@sku.ac.ir

^a Ph.D.

types have attracted increasing attention in recent years. When composites are reinforced with graphene sheets, Shen introduced a novel class of composites which are composed of laminates and each lamina is reinforced by graphene. When volume fraction of graphene sheets are different in each layer, a piecewise functionally graded pattern is revealed. In this case of reinforced composites properties are obtained using a refined micromechanical rule which is calibrated using the data of molecular dynamics simulations. The weight fraction of graphene sheets in this model varies from 3 to 11 percent and temperature dependency of the constituents is included. Stability behaviour of beams, plates and shells reinforced with graphene sheets is well-documented in the open literature. Among them, Kiani and Mirzaei (2018) applied the conventional Ritz method to analyse the buckling and postbuckling of functionally graded graphene reinforced composite (FG-GRC) beams resting on two parameter elastic foundation. Shen *et al.* (2017a) applied the two step perturbation technique to analyse the thermal postbuckling of GRC beams resting on two parameters elastic foundation by means of the third order shear deformation beam theory. Shen *et al.* (2017b) analysed the buckling and postbuckling behaviour of FG-GRC rectangular plates under uniform compressive loads by means of the two step perturbation technique. The developed formulation of this study is applicable to plates which are simply supported all around. Shen *et al.* (2018) also analysed the thermal postbuckling response of rectangular plates subjected to uniform heating by means of the two step perturbation technique. The effect of the Pasternak elastic foundation is also included in this investigation. In another study, Yu *et al.* (2018) also investigated the application of GRC laminates as face sheets in sandwich plates. They analysed the postbuckling response of rectangular plates under mechanical and thermal loads. They showed that, buckling load of sandwich plates with FG-GRC face sheets may be enhanced when the volume fraction of graphene is increased in the face sheets. Mirzaei and Kiani (2017) developed an isogeometric formulation to analyse the thermal buckling of GRC laminated plates with different combinations of boundary conditions. The developed solution method of this research may be used for arbitrary combinations of boundary conditions. To analyse the thermal postbuckling response of FG-GRC rectangular plates, Kiani (2018a) developed a higher order NURBS-based isogeometric formulation for rectangular plates with arbitrary combinations of boundary conditions. It is highlighted that when inner layers of the plate are enriched with maximum graphene sheets, the critical buckling temperature of the plate decreases. Shen and his co-authors (Shen *et al.* 2018, Shen and Xiang 2018a, b) also investigated the buckling of cylindrical panels and shells subjected to different loads in thermal environment. In these works, it is shown that to increase the buckling loads of the shells and decrease the postbuckling deflections, the layers which have the maximum distance with neutral surface of the structure should be enriched with the maximum amount of graphene sheets. Kiani (2019) also investigated the effect of graphene sheet pattern on the buckling of nanocomposite conical shells reinforced with

graphene sheets. The effect of thermal environment is also included in this research. It is shown that, buckling load of the shell decreases significantly when temperature elevates.

In another class, graphene platelets are inserted into the matrix of the composite media. In this case of reinforced composites, properties are obtained using the Halpin-Tsai micromechanical rule. The weight fraction of graphene sheets in this model is less than 1 percent and properties are assumed to be independent of the temperature. The main works on the stability of composite beams, plates and shells reinforced with graphene platelets are as follows. Yang *et al.* (2017) analysed the buckling and postbuckling of functionally graded graphene platelets reinforced composite (FG-GPLRC) beams by means of the first order shear deformation beam theory and differential quadrature method. Elastic properties of the beams are estimated by means of the Halpin-Tsai rule. Yang *et al.* (2018b) investigated the nonlinear in-plane instability of FG-GPLRC shallow arches using an analytical method. In this research, both of the bifurcation and snap-through types of instability are taken into account. The nonlinear prebuckling deformation for bifurcation analysis are also included into the formulation. Kitipornchai *et al.* (2017) applied the conventional Ritz method to analyse the elastic buckling of nanocomposite beams reinforced with FG-GPLs. It is shown that, non-uniform and symmetric distributions of porosity and graphene can achieve the best structural performance. Song *et al.* (2017) applied the single term Galerkin solution method to investigate the buckling and post-buckling of axially compressed rectangular plates. In this research, only simply supported plates are analysed. Applying the two dimensional differential quadrature method, first order shear deformation plate theory and Halpin-Tsai micro-mechanical rule, Wu *et al.* (2017) investigated the thermal buckling and postbuckling of FG-GPLRC rectangular plates. It is shown that, the effect of weight fraction of graphene platelets on critical buckling temperature and thermal postbuckling of uniform FG-GPLRC is almost negligible. Song *et al.* (2018) applied the classical Navier solution method to analyse the buckling of FG-GPLRC rectangular plates within the framework of first order shear deformation plate theory. As shown in this research, a multilayer plate consisting of 10-15 layers is an excellent approximation for the desired functionally graded plate with a continuous through-thickness variation in GPL distribution. Yang *et al.* (2018a) applied the Chebyshev-Ritz formulation to analyse the buckling of FG-GPLRC rectangular plates. The effect of cut-out on the buckling of compressed cylindrical shells made of FG-GPLRC is investigated by Wang *et al.* (2018a). The solution method is based on the finite elements simulation. As shown, larger sized GPLs with fewer single graphene layers are favourable reinforcing fillers in enhancing the buckling performance of the structures. The effect of cut-out on the torsional buckling of FG-GPLRC cylindrical shell is also investigated by Wang *et al.* (2018b). The solution method of this research is based on a finite elements simulation. As shown in this research, square shaped GPLs with fewer layers are preferred as reinforcements for torsional buckling. Wang *et al.* (2018c) also investigated the effect of

GPLs on the nanocomposites subjected to axial compression using the finite elements simulations.

As the above literature survey indicates and to the best of the present authors' knowledge, the only available work on the thermal buckling and postbuckling of FG-GPLRC rectangular plates belongs to Wu *et al.* (2017). In this research, the first order shear deformation plate theory is used for plates which contains clamped and simply supported edges. The governing equations are solved using the generalised differential quadrature method. Present work, however uses the third order shear deformation plate theory which does not require the shear correction factor. Furthermore the solution method is based on the NURBS-based isogeometric formulation suitable for clamped, simply and sliding supported edges. In the present investigation, thermal buckling and postbuckling response of multi-layer graphene platelet reinforced composite plate is investigated. Different patterns of functionally graded for graphene reinforcements is assumed into the formulation. A higher order plate theory, von Kármán type of nonlinearity, Halpin-Tsai micromechanical rule and the NURBS-based isogeometric formulation are used to obtain the basic governing equations dealing with the postbuckling and buckling of FG-GPLRC plates subjected to uniform heating. The developed formulation may be used for arbitrary combinations of boundary conditions. A direct displacement control strategy is applied to the nonlinear equilibrium equations to trace the postbuckling equilibrium path of the plate. It is shown that, for a specific pattern of FG distribution of GPLs, increasing the weight fraction of GPLs enhances the critical buckling temperature of the nanocomposite plate and decreases the thermal postbuckling deflection.

2. Basic formulation

A multilayer composite laminated plate with N_L layers, total thickness h , length a and width b is considered in the current research. All plies are considered to be unified in thickness. Therefore the thickness of each ply is obtained as h/N_L . Each ply is made from a polymeric matrix which is reinforced by graphene platelets. The volume fraction of graphene in each ply may be different. When volume fraction of graphene in layers is different, a piecewise functionally graded graphene reinforced composite laminated plate is achieved.

A Cartesian coordinate system is assigned to the mid-surface corner of the plate where the x axis is through the length, y axis is through the width and z axis is through the thickness.

A third order shear deformation plate theory, known as Reddy's shear deformation plate theory is used in the current investigation to estimate the displacement components of the plate. The theory considers the parabolic variation of shear strains while ignores the thickness stretching. Also the constraint of zero shear strains are satisfied on the top and bottom surfaces of the plate. According to this theory, displacement field is expressed as

$$\mathbf{u} = \mathbf{u}_1 + z\mathbf{u}_2 + f(z)\mathbf{u}_3 \quad (1)$$

In Eq. (1), $\mathbf{u} = \{u, v, w\}^T$. Here, u, v and w denote the displacements through the x, y and z directions, respectively. Also $\mathbf{u}_1 = \{u_0, v_0, w_0\}^T$ indicates the displacements of the mid-surface of the plate. The other vectors are $\mathbf{u}_2 = -\{w_{0,x}, w_{0,y}, 0\}^T$ and $\mathbf{u}_3 = \{\beta_x, \beta_y, 0\}^T$. Here β_x and β_y are the cross section rotations about y and x axes, respectively. It is of worth-noting that, the function $f(z)$ is equal to $f(z) = z(1 - 4z^2/3h^2)$ which satisfies the condition of zero shear strains at the top and bottom surfaces of the plate.

Suitable for nonlinear stability analysis of plates, von Kármán type of strain field are used in this research. This type of strain is compatible with small strains, large deflection and moderate rotations. The components of von Kármán strains in Cartesian coordinate system takes the form

$$\begin{Bmatrix} \epsilon_x \\ \epsilon_y \\ \gamma_{xy} \\ \gamma_{xz} \\ \gamma_{yz} \end{Bmatrix} = \begin{Bmatrix} u_{,x} \\ v_{,y} \\ u_{,y} + v_{,x} \\ u_{,z} + w_{,x} \\ v_{,y} + w_{,y} \end{Bmatrix} + \frac{1}{2} \begin{Bmatrix} w_{,x}^2 \\ w_{,y}^2 \\ 2w_{,x}w_{,y} \\ 0 \\ 0 \end{Bmatrix} \quad (2)$$

Substitution of Eqs (1) into Eq. (2) results in the following expressions for the strain field within the plate

$$\begin{Bmatrix} \boldsymbol{\epsilon} \\ \boldsymbol{\gamma} \end{Bmatrix} = \begin{Bmatrix} \boldsymbol{\epsilon}_m \\ 0 \end{Bmatrix} + \begin{Bmatrix} z\boldsymbol{\kappa}_1 \\ \mathbf{0} \end{Bmatrix} + \begin{Bmatrix} f(z)\boldsymbol{\kappa}_2 \\ f'(z)\boldsymbol{\beta} \end{Bmatrix} \quad (3)$$

where the newly defined functions in Eq. (3) are as

$$\boldsymbol{\epsilon}_m = \begin{Bmatrix} u_{0,x} \\ v_{0,y} \\ u_{0,y} + v_{0,x} \end{Bmatrix} + \frac{1}{2} \begin{Bmatrix} w_{0,x}^2 \\ w_{0,y}^2 \\ 2w_{0,x}w_{0,y} \end{Bmatrix} = \boldsymbol{\epsilon}_L + \boldsymbol{\epsilon}_{NL}, \quad (4)$$

$$\boldsymbol{\kappa}_1 = -\begin{Bmatrix} w_{0,xx} \\ w_{0,yy} \\ 2w_{0,xy} \end{Bmatrix}, \quad \boldsymbol{\kappa}_2 = \begin{Bmatrix} \beta_{x,x} \\ \beta_{y,y} \\ \beta_{x,y} + \beta_{y,x} \end{Bmatrix}, \quad \boldsymbol{\beta} = \begin{Bmatrix} \beta_x \\ \beta_y \end{Bmatrix}$$

The nonlinear part of the strain tensor from Eq. (4) may be expressed in terms of the slope vector as

$$\boldsymbol{\epsilon}_{NL} = \frac{1}{2} A_\theta \boldsymbol{\theta} = \frac{1}{2} \begin{bmatrix} w_{0,x} & 0 \\ 0 & w_{0,y} \\ w_{0,y} & w_{0,x} \end{bmatrix} \begin{Bmatrix} w_{0,x} \\ w_{0,y} \end{Bmatrix} \quad (5)$$

Material of the plate is assumed to be linear and thermoelastic. Therefore the constitutive law for the plate may be expressed as

$$\begin{aligned} \boldsymbol{\sigma} &= \mathbf{C}(\boldsymbol{\epsilon} - \boldsymbol{\epsilon}_T) \\ \boldsymbol{\tau} &= \mathbf{G}\boldsymbol{\gamma} \end{aligned} \quad (6)$$

where the following definitions apply

$$\begin{aligned} \boldsymbol{\sigma} &= \begin{Bmatrix} \sigma_x \\ \sigma_y \\ \sigma_{xy} \end{Bmatrix}, \quad \boldsymbol{\epsilon}_T = \Delta T \begin{Bmatrix} \alpha_{11} \\ \alpha_{22} \\ \alpha_{12} \end{Bmatrix}, \quad \boldsymbol{\tau} = \begin{Bmatrix} \tau_{xz} \\ \tau_{yz} \end{Bmatrix} \\ \mathbf{C} &= \begin{bmatrix} Q_{11} & Q_{12} & Q_{16} \\ Q_{12} & Q_{22} & Q_{26} \\ Q_{16} & Q_{26} & Q_{66} \end{bmatrix}, \quad \mathbf{G} = \begin{bmatrix} Q_{44} & Q_{45} \\ Q_{45} & Q_{55} \end{bmatrix} \end{aligned} \quad (7)$$

It is assumed that each layer of the composite plate is isotropic. Therefore the stiffness components in Eq. (7) of the plate may be expressed in terms of elasticity modulus E and Poisson's ratio ν of the layer as

$$\begin{aligned} Q_{11} = Q_{22} &= \frac{E}{1-\nu^2}, \quad Q_{12} = \frac{\nu E}{1-\nu^2}, \quad Q_{16} = Q_{26} = 0 \\ Q_{44} = Q_{55} = Q_{66} &= \frac{E}{2(1+\nu)}, \quad Q_{45} = 0 \end{aligned} \quad (8)$$

The membrane stress resultants, \mathbf{N} , The membrane out-of-plane shear stress resultants, \mathbf{Q} and the bending stress resultants, \mathbf{M} may be obtained upon integration of stress components (6) as

$$\begin{pmatrix} \mathbf{N} \\ \mathbf{M} \\ \mathbf{P} \\ \mathbf{Q} \end{pmatrix} = \begin{bmatrix} \mathbf{A} & \mathbf{B} & \mathbf{E} & \mathbf{0} \\ \mathbf{B} & \mathbf{D} & \mathbf{F} & \mathbf{0} \\ \mathbf{E} & \mathbf{F} & \mathbf{H} & \mathbf{0} \\ \mathbf{0} & \mathbf{0} & \mathbf{0} & \mathbf{0} \end{bmatrix} \begin{pmatrix} \boldsymbol{\varepsilon}_m \\ \boldsymbol{\kappa}_1 \\ \boldsymbol{\kappa}_2 \\ \boldsymbol{\beta} \end{pmatrix} - \begin{pmatrix} \mathbf{N}_T \\ \mathbf{M}_T \\ \mathbf{P}_T \\ \mathbf{0} \end{pmatrix} \quad (9)$$

where in a compact form may be expressed as

$$\hat{\boldsymbol{\sigma}} = \hat{\mathbf{D}}\hat{\boldsymbol{\varepsilon}} - \hat{\boldsymbol{\sigma}}_0 \quad (10)$$

The stiffness matrices of the composite media in Eq. (9) are obtained as

$$\begin{aligned} &(\mathbf{A}, \mathbf{B}, \mathbf{D}, \mathbf{E}, \mathbf{F}, \mathbf{H}, \mathbf{D}^s) = \\ &\sum_{k=1}^{N_L} \int_{h_{k-1}}^{h_k} (\mathbf{C}, z\mathbf{C}, z^2\mathbf{C}, f(z)\mathbf{C}, zf(z)\mathbf{C}, f^2(z)\mathbf{C}, f'^2(z)\mathbf{G}) dz \end{aligned} \quad (11)$$

and the thermally induced force and moment resultants appeared in Eq. (9) are evaluated by

$$(\mathbf{N}_T, \mathbf{M}_T, \mathbf{P}_T) = \sum_{k=1}^{N_L} \int_{h_{k-1}}^{h_k} \mathbf{A}_T \Delta T(1, z, f(z)) dz \quad (12)$$

where in Eq. (12)

$$\mathbf{A}_T = \mathbf{C} \begin{bmatrix} 1 & 0 \\ 0 & 1 \\ 0 & 0 \end{bmatrix} \begin{bmatrix} \alpha \\ \alpha \\ 0 \end{bmatrix} \quad (13)$$

It is assumed that the composite laminated plate consists of even number of layers, i.e., N_L . As mentioned earlier, the volume fraction of GPLs in each layer may be different. Three different types of volume fraction distribution for FG-GPLRCs is considered in this research which are FG-O, FG-X and UD. Distribution of volume fraction for each layer is according to the following expressions

$$\begin{aligned} \text{UD: } V_{GPL}^{(k)} &= V_{GPL}^* \\ \text{FG-X: } V_{GPL}^{(k)} &= 2V_{GPL}^* \frac{|2k - N_L - 1|}{N_L} \\ \text{FG-O: } V_{GPL}^{(k)} &= 2V_{GPL}^* \left(1 - \frac{|2k - N_L - 1|}{N_L}\right) \end{aligned} \quad (14)$$

where in Eq. (14), $V_{GPL}^{(k)}$ indicates the volume fraction of GPLs in the k -th layer of the laminate. In Eq. (14) k takes

the values from 1 to N_L . Also V_{GPL}^* indicates the total volume fraction of the GPLs in the plate. The total volume fraction of GPLs may be expressed in terms of the weight fraction of the GPLs in the whole plate, W_{GPL} and also the mass density of the constituents, ρ_m and ρ_{GPL} as

$$V_{GPL}^* = \frac{W_{GPL}}{W_{GPL} + \frac{\rho_{GPL}}{\rho_m}(1 - W_{GPL})} \quad (15)$$

It is known that the size and geometry of the fillers are two important factors for the estimation of properties of polymer composites. To estimate the elasticity modulus of the GPLRCs in this research, the Halpin-Tsai rule is used. This rule is widely accepted in the estimation of elasticity modulus of GPLRCs (Yang *et al.* 2017, 2018a, b). According to this micromechanical rule, the elasticity modulus of each layer of the composite may be obtained as

$$E = \frac{3}{8} \frac{1 + \xi_L \eta_L V_{GPL}}{1 - \eta_L V_{GPL}} E_m + \frac{5}{8} \frac{1 + \xi_T \eta_T V_{GPL}}{1 - \eta_T V_{GPL}} E_m \quad (16)$$

where the auxiliary parameters η_L and η_T in Eq. (16) are expressed as

$$\eta_L = \frac{E_{GPL} - E_m}{E_{GPL} + \xi_L E_m} \quad \eta_T = \frac{E_{GPL} - E_m}{E_{GPL} + \xi_T E_m} \quad (17)$$

In Eq. (17), E_m and E_{GPL} are the elasticity modulus of the isotropic matrix and isotropic GPLs, respectively. The geometrical factors of GPLs are obtained in terms of the thickness of the GPLs, t_{GPL} , width of the GPLs, b_{GPL} and length of the GPLs, a_{GPL} as follows

$$\xi_L = \frac{a_{GPL}}{t_{GPL}} \quad \xi_T = \frac{b_{GPL}}{t_{GPL}} \quad (18)$$

The thermal expansion coefficient of the composite media α and Poisson's ratio of the composite media ν may be obtained easily by means of the properties of the constituents according to the simple rule of mixtures. Accordingly one may write (Cong *et al.* 2018, Duc and Nguyen 2017, Duc *et al.* 2017a, b, Thanh *et al.* 2016, Thom *et al.* 2017, Voung and Duc 2018)

$$\begin{aligned} \alpha &= \alpha_m V_m + \alpha_{GPL} V_{GPL} \\ \nu &= \nu_m V_m + \nu_{GPL} V_{GPL} \end{aligned} \quad (19)$$

In Eq. (19), the subscripts m and GPL represent the matrix and GPLs respectively. The virtual displacement principle which is also known as the static version of the Hamilton principle may be used to obtain the governing equations of a composite laminated plate subjected to thermal loading. Since external forces are absent, the total energy of the plate is equal to the strain energy of the plate. Therefore in an equilibrium position one may write

$$\delta \Pi = \delta U = \int_{\Omega} \delta \hat{\boldsymbol{\varepsilon}}^T \hat{\boldsymbol{\sigma}} d\Omega = 0 \quad (20)$$

3. Solution method; Isogeometric Analysis

The isogeometric finite elements formulation is applied recently to different problems of applied mechanics. In the next, a summary of the method is only introduced. For more details on the process one may refer to the primary investigation of Hughes *et al.* (2005) or Atri and Shojaee (2018) and Roodsarabi *et al.* (2016).

In one dimensional space, a knot vector consists of a non-decreasing set of numbers, i.e., $k(\xi) = \{\xi_1, \xi_2, \xi_3, \dots, \xi_{n+p+1}\}$. According to the condition of non-decreasing set of numbers for any integer number i , $\xi_i \leq \xi_{i+1}$. All of the numbers satisfy the condition $0 \leq \xi_i \leq 1$ where ξ_i is the i -th knot. Also in the definition of knot, n and p stand for the number of basis functions and the order of the B-spline basis function, respectively. With the aid of a given knot vector $k(\xi)$, the B-spline basis function is defined according to the following recursive Cox-de Boor formula

$$N_{i,0}(\xi) = \begin{cases} 1 & \xi_i \leq \xi < \xi_{i+1} \\ 0 & \text{else} \end{cases} \quad (21)$$

$$N_{i,p}(\xi) = \frac{\xi - \xi_i}{\xi_{i+p} - \xi_i} N_{i,p-1}(\xi) + \frac{\xi_{i+p+1} - \xi}{\xi_{i+p+1} - \xi_{i+1}} N_{i+1,p-1}(\xi)$$

It is of worth noting that, in the above equation, the value of 0/0 is set equal to zero. For two dimensional domains, such as plates and shells, the base functions may be determined using the tensor product of two one dimensional B-spline functions. These functions are obtained as

$$R_{i,j}^{p,q} = \frac{N_{i,p}(\xi)N_{j,q}(\eta)w_{i,j}}{\sum_{i=1}^n \sum_{j=1}^m N_{i,p}(\xi)N_{j,q}(\eta)w_{i,j}} \quad (22)$$

Where in Eq. (22), the shape function of order p in ξ direction and of order q in η direction are denoted respectively by $N_{i,p}(\xi)$ and $N_{j,q}(\eta)$. It should be mentioned that derivation of the shape functions $N_{j,q}(\eta)$ is similar to shape functions $N_{i,p}(\xi)$ which is provided in Eq. (21). In derivation of the shape functions $N_{j,q}(\eta)$ the knot vectors k_η should be used. Furthermore, $w_{i,j}$ represent the weight coefficients.

The displacement approximation within the plate domain using the NURBS takes the form

$$\begin{aligned} & (u_{0i}^h, v_{0i}^h, w_{0i}^h, \beta_{xi}^h, \beta_{yi}^h) \\ & = \sum_{i=1}^{nm} R_i(\mathbf{x})(u_{0i}, v_{0i}, w_{0i}, \beta_{xi}, \beta_{yi}) \end{aligned} \quad (23)$$

where the definition of $R_i(\mathbf{x})$ is provided in Eq. (22). Furthermore, in Eq. (23), the displacements at the control node i are denoted by (u_i, v_i, w_i) and the rotations at the control node i are denoted by (β_{xi}, β_{yi}) . In a compact form Eq. (23) takes the form

$$\mathbf{u}^h(\mathbf{x}) = \sum_A R_i(\mathbf{x})\mathbf{q}_A \quad (24)$$

Substitution of the above equation into the Eq. (4) results in the expression of strain in terms of vector of nodal degrees of freedom associated with the control point as

$$\hat{\boldsymbol{\varepsilon}} = \left(\mathbf{B}^L + \frac{1}{2} \mathbf{B}^{NL} \right) \mathbf{q} \quad (25)$$

where \mathbf{B}^L is the infinitesimal strain field which may be written as

$$\mathbf{B}_A^L = [(\mathbf{B}_A^m)^T (\mathbf{B}_A^{b1})^T (\mathbf{B}_A^{b2})^T (\mathbf{B}_A^s)^T]^T \quad (26)$$

where the following definitions apply

$$\begin{aligned} \mathbf{B}_A^m &= \begin{bmatrix} R_{A,x} & 0 & 0 & 0 & 0 \\ 0 & R_{A,y} & 0 & 0 & 0 \\ R_{A,y} & R_{A,x} & 0 & 0 & 0 \end{bmatrix} \\ \mathbf{B}_A^{b1} &= - \begin{bmatrix} 0 & 0 & R_{A,xx} & 0 & 0 \\ 0 & 0 & R_{A,yy} & 0 & 0 \\ 0 & 0 & 2R_{A,xy} & 0 & 0 \end{bmatrix} \\ \mathbf{B}_A^{b2} &= \begin{bmatrix} 0 & 0 & 0 & R_{A,x} & 0 \\ 0 & 0 & 0 & 0 & R_{A,y} \\ 0 & 0 & 0 & R_{A,y} & R_{A,x} \end{bmatrix} \\ \mathbf{B}_A^s &= \begin{bmatrix} 0 & 0 & 0 & R_A & 0 \\ 0 & 0 & 0 & 0 & R_A \end{bmatrix} \\ \mathbf{B}_A^g &= \begin{bmatrix} 0 & 0 & R_{A,x} & 0 & 0 \\ 0 & 0 & R_{A,y} & 0 & 0 \end{bmatrix} \end{aligned} \quad (27)$$

Similar to linear strain, the non-linear part of the strain field may be expressed as

$$\mathbf{B}_A^{NL}(\mathbf{q}) = \mathbf{A}_\theta \mathbf{B}_A^g \quad (28)$$

Recalling the definition of the strain field from Eq. (25), the variation of the strain field may be expressed as

$$(\mathbf{K}_L + \mathbf{K}_{NL} - \mathbf{K}_G)\mathbf{q} = 0 \quad (29)$$

where in the above equations, \mathbf{K}_L , \mathbf{K}_{NL} and \mathbf{K}_G are, respectively, the linear, nonlinear and geometrical stiffness matrices. These matrices may be evaluated by

$$\begin{aligned} \mathbf{K}_L &= \int_{\Omega} (\mathbf{B}^L)^T \widehat{\mathbf{D}} \mathbf{B}^L d\Omega \\ \mathbf{K}_{NL} &= \frac{1}{2} \int_{\Omega} (\mathbf{B}^L)^T \widehat{\mathbf{D}} \mathbf{B}^{NL} d\Omega + \int_{\Omega} (\mathbf{B}^{NL})^T \widehat{\mathbf{D}} \mathbf{B}^L d\Omega \\ & \quad + \frac{1}{2} \int_{\Omega} (\mathbf{B}^{NL})^T \widehat{\mathbf{D}} \mathbf{B}^{NL} d\Omega \\ \mathbf{K}_G &= \int_{\Omega} (\mathbf{B}^g)^T \begin{bmatrix} N_{xT} & 0 \\ 0 & N_{yT} \end{bmatrix} \mathbf{B}^g d\Omega \end{aligned} \quad (30)$$

It is of worth-noting that, even under uniform temperature rise, a rectangular plate may not follow the classical thermal postbuckling behaviour. Boundary conditions and lamination scheme both affect the nonlinear thermal stability of the plate. When all edges of the plate are of clamped type, for both the symmetric and asymmetric lamination schemes, thermal bifurcation takes place. However, when at least one edge of the plate is of the

simply supported type, thermal bifurcation and regular postbuckling happens only for symmetric lamination scheme. In this study, only the classical postbuckling equilibrium path of the plate is considered.

For the numerical integration, the standard Gaussian rules are used in this work without the need for any special calculations.

It should be mentioned that Eq. (29) is a non-linear eigenvalue problem which should be solved according to a displacement control strategy. For the sake of brevity, the process of solution is not mentioned in here, meanwhile readers of this study may refer to the previous investigations of the author, see e.g., (Kitipornchai *et al.* 2017, Kiani 2017, 2018b, c).

4. Numerical result and discussion

In the present research, thermal buckling and postbuckling response of FG-GPLRC rectangular plates is investigated by means of the third order shear deformation plate theory and NURBS-based isogeometric formulation. In all numerical calculations, the cubic order NURBS basis functions are used and a 4×4 Gaussian quadrature scheme is used for integration of each element. Each side of the plate may be clamped (C), simply supported (S) or sliding supported (X). For a clamped plate, all of the displacements, normal derivative of lateral deflection and both of the rotations are restrained at the support. For a simply supported edge, all of the displacement and tangential rotation are restrained at the support. For a sliding supported edge, the in-plane displacements and the normal rotation are equal to zero.

Many factors affect the response of the composite laminated plate reinforced with GPLs. The geometry and dimensions of GPLs is one of the main factors. Wu *et al.* (2017) performed a series of studies on the influence of geometrical parameters of GPLs on thermal buckling and post-buckling of FG-GPLRC rectangular plates. The effects of a_{GPL}/b_{GPL} and b_{GPL}/t_{GPL} on the thermal buckling and postbuckling of FG-GPLRC is examined. It is shown that for values of b_{GPL}/t_{GPL} greater than 1000, the value of critical buckling temperature almost remains constant. Also in another study by Wu *et al.* (2017) it is shown that the post-buckling curves of UD, FG-X and FG-O plates are hardly dependent to a_{GPL}/b_{GPL} . Therefore in all of the numerical results on this study the following geometrical parameters which are proposed by Wu *et al.* (2017) are used. The geometrical properties of GPLs are as follows $a_{GPL} = 2.5 \mu\text{m}$, $b_{GPL} = 1.5 \mu\text{m}$ and $t_{GPL} = 1.5 \text{ nm}$.

The other important factor which affects the thermal buckling and post-buckling response of FG-GPLRC rectangular plates is the number of layers. Wu *et al.* (2017) performed an investigation on the effect of number of layers. Their results also confirm that for the number of layers larger than 10, the critical buckling temperature almost remains constant and also thermal post-buckling deflection is unchanged. Therefore in the current investigation, for all of the numerical results, the number of layers is set equal to $N_L = 10$.

Table 1 Thermo-mechanical properties of the matrix and GPLs (Wu *et al.* 2017)

Properties	Epoxy	GPL
Elasticity modulus (E)[GPa]	3.0	1010
Mass density (ρ) [kg/m ³]	1200	1062.5
Thermal expansion coefficient ($\times 10^{-6}/\text{K}$)	60	5.0
Poisson's ratio (ν)	0.34	0.186

The following convention is used to distinguish the boundary condition of the plate. A four letter phrase is used for each class of boundary condition where the first letter is associated to $x = 0$, the second letter is associated to $y = 0$, the third letter indicates the boundary on $x = a$ and the fourth letter is the boundary on $y = b$.

For the numerical results of this study, unless otherwise stated, the thermo-mechanical properties of epoxy and graphene platelets are taken from Wu *et al.* (2017) and are listed in Table 1.

In whole of the post-buckling results, the center point deflection of the plate is denoted by W .

4.1 Comparison Studies

In this section two comparison studies are given. A comparison study is presented between the numerical results of our study with those obtained by Wu *et al.* (2017). In the present study a third order shear deformation plate theory is used and solution method is based on the NURBS-based isogeometric formulation. However in the analysis of Wu *et al.* (2017), the first order shear deformation plate theory is used and the solution method is based on the two dimensional differential quadrature. Comparison is provided in Table 2. It is seen that our results are in excellent agreement with those of Wu *et al.* (2017) which accepts the accuracy and effectiveness of our solution method.

In another comparison study, the thermal post-buckling equilibrium path of square plates is compared with the available data in the open literature. In this comparison, a single layer isotropic plate is considered and results are compared with those of Raju and Rao (1988). For this comparison study, a thin square plate is considered. The

Table 2 A comparison on critical buckling temperature difference ΔT_{cr} [K] of square SSSS FG-GPLRC plates with $W_{GPL} = 0.3\%$, various thickness ratios and graded patterns

Pattern	Source	$a/h = 25$	$a/h = 35$	$a/h = 45$
UD	Present	32.517	16.672	10.106
	Wu <i>et al.</i> (2017)	32.539	16.679	10.109
FG-X	Present	40.230	20.650	12.524
	Wu <i>et al.</i> (2017)	40.261	20.660	12.528
FG-O	Present	24.804	12.703	7.696
	Wu <i>et al.</i> (2017)	24.817	12.707	7.698

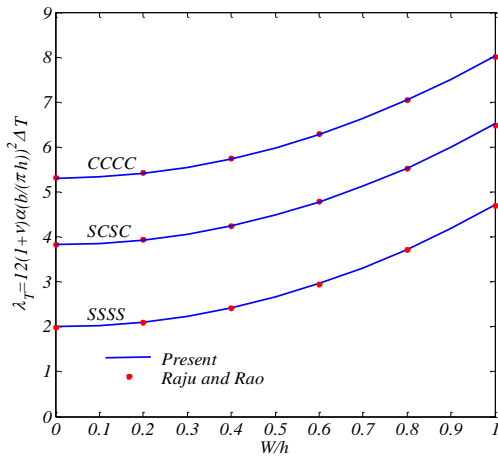


Fig. 1 Comparison of thermal postbuckling of square thin plates with those of Raju and Rao (1988) for different types of boundary conditions

side to thickness ratio is set equal to $a/h = 100$. Three different types of boundary conditions are assumed and comparison is shown in Fig. 1. It is concluded that, our results match well with the available data in the open literature which shows the accuracy and correctness of our solution method and formulation.

4.2 Parametric studies

After validating the proposed solution method and formulation, novel numerical results are given in this section.

Critical buckling temperature of FG-GPLRC plates are obtained for different combinations of boundary conditions and graded patterns. Results of this study are provided in Fig. 2. Four different combinations of boundary conditions are assumed which are SSSS, CCCC, SCSC and XCXC. For each case, the critical buckling temperature is obtained as a function of weight fraction of GPLs. It is seen that for all combinations of boundary conditions, in UD plates as the weight fraction of GPLs increases, the critical buckling temperature almost remains unchanged. For FG-X plates, on the other hand, critical buckling temperature increases permanently with the increase in the weight fraction of GPLs. Finally for the third FG pattern which is FG-O, enrichment of the composite media with more GPLs, results in the lower critical buckling temperature. Such trends are also reported by Wu *et al.* (2017). In general when the composite plate is reinforced with more GPLs, the stiffness of the plate increases. However according to Eq. (12), the critical buckling temperature of the plate may remain constant, or increase/decrease versus the weight fraction of GPLs. The critical buckling temperature of the plate

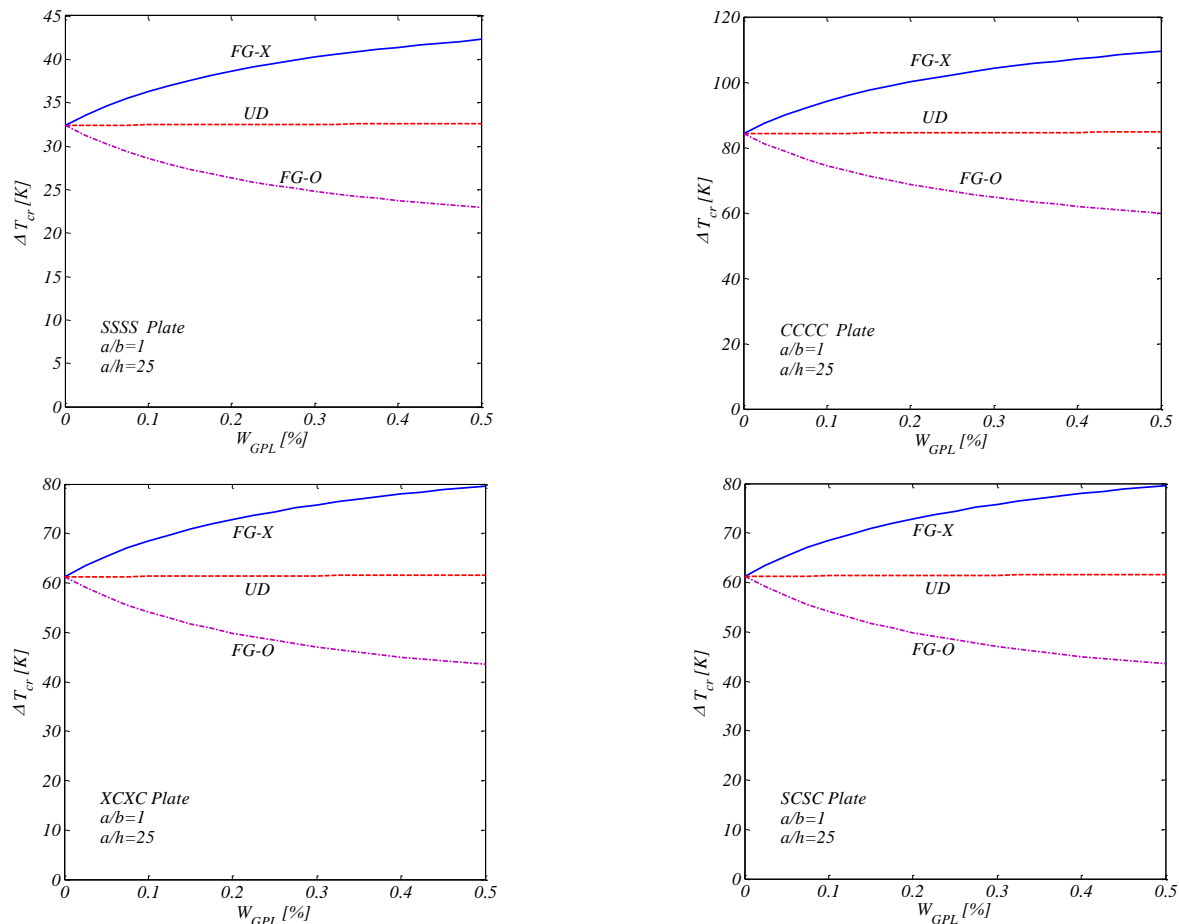


Fig. 2 Influences of graded pattern and weight fraction of GPLs on the critical buckling temperature of different FG-GPLRC rectangular plates

depends on both the stiffness of the plate and the thermal stiffness. Since increasing the weight fraction of GPLs results in increasing both of these stiffnesses, their ratio may increase, decrease or remain constant. Further examination of the results of this figure indicates that CCCC plates have the highest critical buckling temperature. When a clamped edge is replaced by a simply supported edge, critical buckling temperature decreases. This is expected since in clamped edges the local flexural rigidity of the support is much more than the simply supported plates.

Fig. 3 provides the critical buckling temperature and the buckled shape of FG-GPLRC plates. In this example, different combinations of boundary conditions are taken into account. Square plates with thickness ratio $a/h = 25$ are assumed. The weight fraction of the GPLs is set equal to

$W_{GPL} = 0.3\%$ and FG-X pattern is assumed for the lamination scheme. It is seen that the essential boundary conditions are fully satisfied at the supports in the buckled shapes of the plate. When one edge of the plate changes from clamped to sliding supported, the critical buckling temperature decreases significantly due to the ability of the edge to move laterally.

Postbuckling equilibrium path of a class of FG-GPLRC plates is provided in Fig. 4. In this figure, plates with aspect ratio $a/b = 1$ are considered. Thickness ratio of the plate is set equal to $a/h = 25$. Three different types of boundary conditions are considered which are CCCC, SSSS and SCSC. The weight fraction of the GPLs is also set equal to $W_{GPL} = 0.3\%$. It is seen that, for all cases of boundary conditions, FG-X plates have higher critical buckling temperature than UD case. Also the UD case has the higher

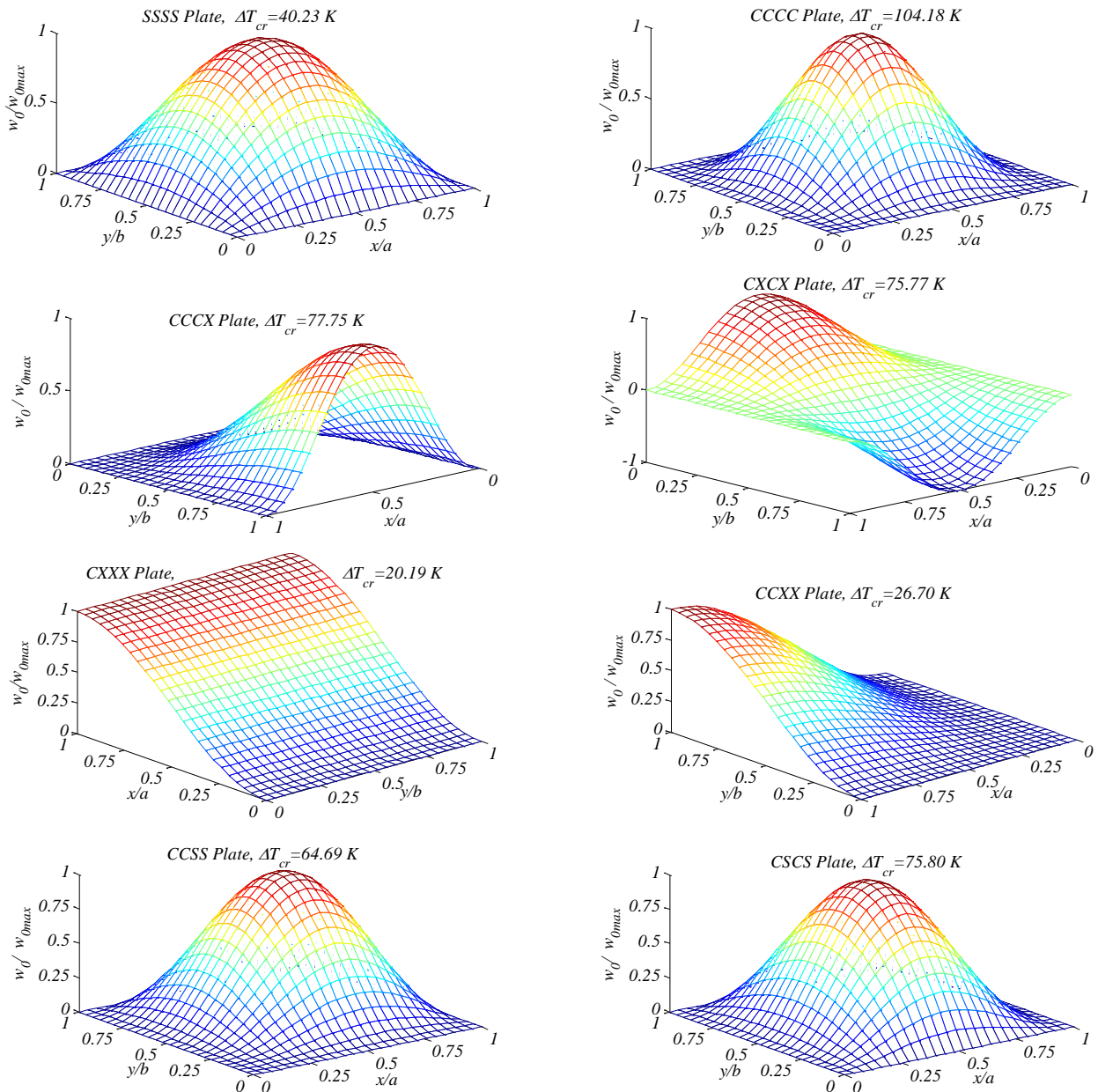


Fig. 3 Critical buckling temperature and buckled configurations of FG-X GPLRC plates with $a/b = 1$, $a/h = 25$, $W_{GPL} = 0.3\%$ and different types of boundary conditions

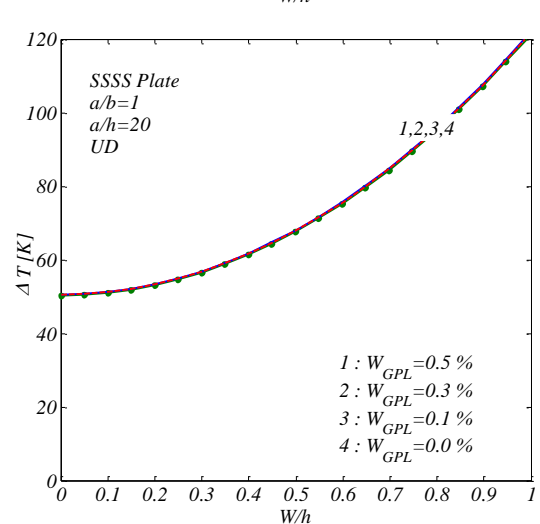
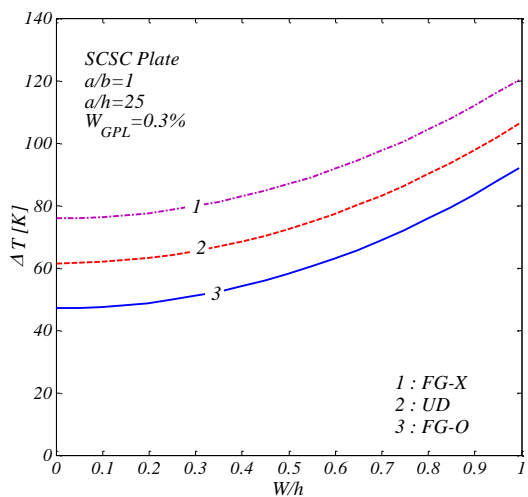
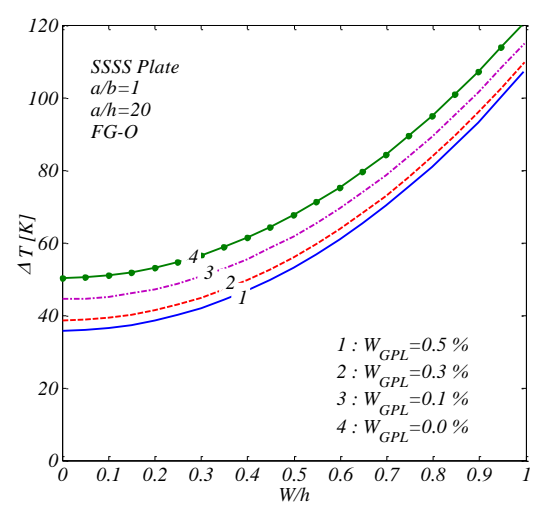
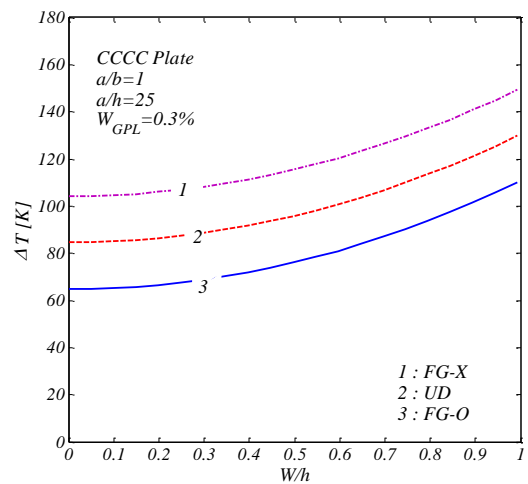
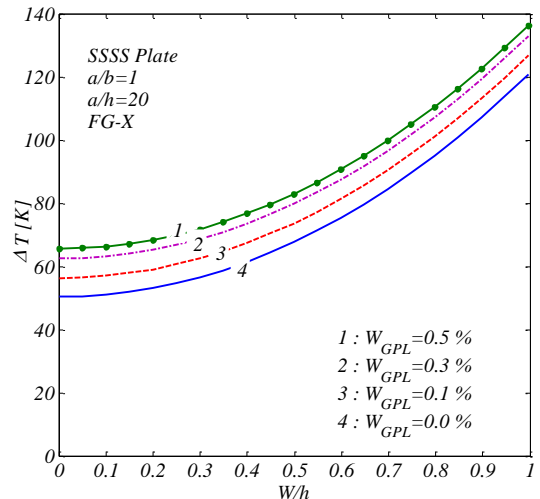
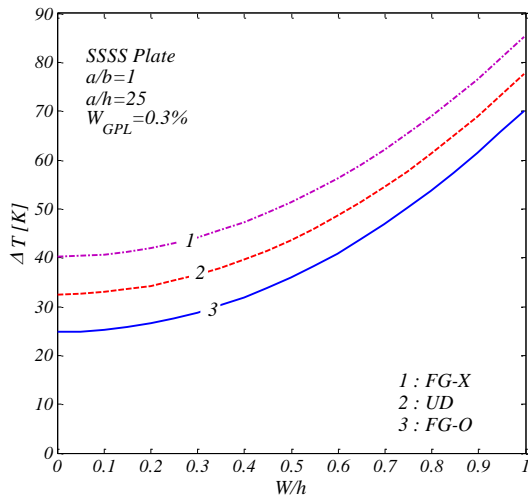


Fig. 4 Thermal postbuckling response of FG-GPLRC plates with different boundary conditions and graded patterns

Fig. 5 The influence of weight fraction of GPLs on the thermal postbuckling of FG-GPLRC plates

critical buckling temperature than the FG-O plate. The post-buckling equilibrium path of FG-GPLRC plates is unique and stable. Following the bifurcation buckling of FG-GPLRCs, the maximum post-buckling deflection belongs to FG-O plates and the minimum one belongs to FG-X plates. Post-buckling deflection of UD plates, serves as an

intermediate response for FG-X and FG-O plates. In FG-X plates, the surfaces which are closed to the free surfaces of the plate are enriched with more volume fraction of GPL which results in the higher flexural rigidity of the plate. Thus higher critical buckling temperatures and lower post-buckling deflections are concluded.

The influence of weight fraction of GPLs on the thermal postbuckling behaviour of FG-GPLRC plates is depicted in Fig. (5). In this figure, plates in square shape with $a/h = 20$ are considered. Different functionally graded patterns are considered. In each case, four different weight fractions are assumed for the plate. As seen from the results of this figure, increasing the weight fraction of GPLs increases the critical buckling temperature of FGX GPLRCs and therefore diminishes the post-buckling deflection. On the other hand, the behaviour is opposite for FG-O plates. Critical buckling temperature decrease with the increase in the weight fraction of GPLs and higher post-buckling deflections are revealed as the weight fraction of GPLs increases. For UD plates, critical buckling temperature and post-buckling deflection are almost remain unchanged with respect to weight fraction of GPLs. The reason of such behaviour is due to the fact that as the weight fraction of GPLs increases both of the stiffness of the structure and thermal stiffness increase. The ratio of these two parameters may increase, decrease or remains unchanged. As a result, thermal post-buckling temperatures also may decrease, increase or remain unchanged.

5. Conclusions

In the current investigation, the thermal buckling and postbuckling responses of FG-GPLRC rectangular plates is investigated by means of an isogeometric formulation. The developed formulation is based on the third order shear deformation theory, von Kármán type of geometrical nonlinearity and NURBS-based formulation. Properties of the composite media are obtained using the modified Halpin-Tsai approach and are assumed to be independent of temperature. With the aid of virtual displacement principle, the governing equilibrium equations of the plate are obtained. These equations are solved using a direct displacement control formulation. Results of this study indicate that, graded pattern of GPLs is an important factor on critical buckling temperature of the plate. In general, highest critical buckling temperature belongs to FG-X plates which means that lowest post-buckling deflection is associated to FG-X plates. Also weight fraction of GPLs is another important factor. The influence of this factor depends on the FG pattern. In FG-X plate when the weight fraction increases, critical buckling temperature increases and post-buckling deflection diminishes. For FG-O plates, however trends is inverse. In UD plates, critical buckling temperature and post-buckling deflections are almost independent of weight fraction of GPLs.

References

- Atri, H.R. and Shojaee, S. (2018), "Truncated hierarchical B-splines in isogeometric analysis of thin shell structures", *Steel Compos. Struct., Int. J.*, **26**(2), 171-182. <http://dx.doi.org/10.12989/scs.2018.26.2.171>
- Cadelano, E., Palla, P.L., Giordano and S. and Colombo, L. (2009), "Nonlinear elasticity of monolayer graphene", *Physical Review Letters*, **102**, Art No. 235502. <https://doi.org/10.1103/PhysRevLett.102.235502>
- Cong, P.H., Chien, T.M., Khoa, N.D. and Duc, N.D. (2018), "Nonlinear thermomechanical buckling and post-buckling response of porous FGM plates using Reddy's HSDT", *Aerosp. Sci. Technol.*, **77**, 419-428. <https://doi.org/10.1016/j.ast.2018.03.020>
- Das, T.K. and Prusty, S. (2013), "Graphene-based polymer composites and their applications", *Polymer-Plast. Technol. Eng.*, **52**, 319-331. <https://doi.org/10.1080/03602559.2012.751410>
- Duc, N.D. and Nguyen, P.D. (2017), "The dynamic response and vibration of functionally graded carbon nanotubes reinforced composite (FG-CNTRC) truncated conical shells resting on elastic foundation", *Materials*, **10**, Article Number 1194. <https://doi.org/10.3390/ma10101194>
- Duc, N.D., Cong, P.H., Tuan, N.D., Tran, P. and Thanh, N.V. (2017a), "Thermal and mechanical stability of functionally graded carbon nanotubes (FG CNT)-reinforced composite truncated conical shells surrounded by the elastic foundations", *Thin-Wall. Struct.*, **115**, 300-310. <https://doi.org/10.1016/j.tws.2017.02.016>
- Duc, N.D., Quan, T.Q. and Nguyen, D.P. (2017b), "New approach to investigate nonlinear dynamic response and vibration of imperfect functionally graded carbon nanotube reinforced composite double curved shallow shells", *Aerosp. Sci. Technol.*, **71**, 360-372. <https://doi.org/10.1016/j.ast.2017.09.031>
- Hughes, T.J.R., Cottrell, J.A. and Bazilevs, Y. (2005), "Isogeometric analysis: CAD, finite elements, NURBS, exact geometry and mesh refinement", *Comput. Methods Appl. Mech. Eng.*, **194**, 4135-4195. <https://doi.org/10.1016/j.cma.2004.10.008>
- Kiani, Y. (2017), "Thermal Post-Buckling of FG-CNT Reinforced Composite Plates", *Compos. Struct.*, **159**, 299-306. <https://doi.org/10.1016/j.compstruct.2016.09.084>
- Kiani, Y. (2018a), "NURBS-based isogeometric thermal postbuckling analysis of temperature dependent graphene reinforced composite laminated plates", *Thin-Wall. Struct.*, **125**, 211-219. <https://doi.org/10.1016/j.tws.2018.01.024>
- Kiani, Y. (2018b), "Thermal post-buckling of temperature dependent sandwich plates with FG-CNTRC face sheets", *J. Thermal Stress.*, **41**, 866-882. <https://doi.org/10.1080/01495739.2018.1425645>
- Kiani, Y. (2018c), "Isogeometric large amplitude free vibration of graphene reinforced laminated plates in thermal environment using NURBS formulation", *Comput. Methods Appl. Mech. Eng.*, **332**, 86-101. <https://doi.org/10.1016/j.cma.2017.12.015>
- Kiani, Y. (2019), "Buckling of functionally graded graphene reinforced conical shells under external pressure in thermal environment", *Compos. Part B: Eng.*, **159**, 128-137. <https://doi.org/10.1016/j.compositesb.2018.08.052>
- Kiani, Y. and Mirzaei, M. (2018), "Enhancement of non-linear thermal stability of temperature dependent laminated beams with graphene reinforcements", *Compos. Struct.*, **186**, 114-122. <https://doi.org/10.1016/j.compstruct.2017.11.086>
- Kitipornchai, S., Chen, D. and Yang, J. (2017), "Free vibration and elastic buckling of functionally graded porous beams reinforced by graphene platelets", *Mater. Des.*, **116**, 656-665. <https://doi.org/10.1016/j.matdes.2016.12.061>
- Kulkarni, D.D., Choi, I., Singamaneni, S.S. and Tsukruk, V.V. (2010), "Graphene oxide polyelectrolyte nanomembranes", *ACS Nano*, **4**, 4667-4676. <https://doi.org/10.1021/nn101204d>
- Lin, F., Xiang, Y. and Shen, H.S. (2017), "Temperature dependent mechanical properties of graphene reinforced polymer nanocomposites A molecular dynamics simulation", *Compos. Part B: Eng.*, **111**, 261-269. <https://doi.org/10.1016/j.compositesb.2016.12.004>
- Mirzaei, M. and Kiani, Y. (2017), "Isogeometric Thermal buckling

- Analysis of Temperature Dependent FG Graphene Reinforced Laminated Plates using NURBS Formulation”, *Compos. Struct.*, **180**, 606-616. <https://doi.org/10.1016/j.compstruct.2017.08.057>
- Ni, Z., Bu, H., Zou, M., Yi, H., Bi, K. and Chen, Y. (2010), “Anisotropic mechanical properties of graphene sheets from molecular dynamics”, *Physica B: Condensed Matter*, **405**, 1301-1306. <https://doi.org/10.1016/j.physb.2009.11.071>
- Novoselov, K.S., Geim, A.K., Morozov, S.V., Jiang, D., Zhang, Y., Dubonos, S.V., Grigorieva, I.V. and Firsov, I.V. (2004), “Electric field effect in atomically thin carbon films”, *Science*, **306**, 666-669. <https://doi.org/10.1126/science.1102896>
- Parashar, A. and Mertiny, P. (2012), “Representative volume element to estimate buckling behavior of graphene/polymer nanocomposite”, *Nanoscale Res. Lett.*, **7**, 515-520. <https://doi.org/10.1186/1556-276X-7-515>
- Potts, J.R., Dreyer, D.R., Bielawski, C.W. and Ruoff, R.S. (2011), “Graphene-based polymer nanocomposites”, *Polymer*, **52**, 5-25. <https://doi.org/10.1016/j.polymer.2010.11.042>
- Rafiee, M.A., Rafiee, J., Wang, Z., Song, H., Yu, Z. and Koratkar, N. (2009a), “Enhanced mechanical properties of nanocomposites at low graphene content”, *ACS Nano*, **3**, 3884-3990. <https://doi.org/10.1021/nn9010472>
- Rafiee, M.A., Rafiee, J., Yu, Z.Z. and Koratkar, N. (2009b), “Buckling resistant graphene nanocomposites”, *Appl. Phys. Lett.*, **95**, Art No. 223103. <https://doi.org/10.1063/1.3269637>
- Raju, K.K. and Rao, G.V. (1988), “Thermal Postbuckling of a square plate resting on an elastic foundation by finite element method”, *Comput. Struct.*, **28**, 195-199. [https://doi.org/10.1016/0045-7949\(88\)90039-9](https://doi.org/10.1016/0045-7949(88)90039-9)
- Reddy, C.D., Rajendran, S. and Liew, K.M. (2006), “Equilibrium configuration and continuum elastic properties of finite sized graphene”, *Nanotechnology*, **17**, 864-870. <https://doi.org/10.1088/0957-4484/17/3/042>
- Roodsarabi, M., Khatibinia, M. and Sarafrazi, S.R. (2016), “Hybrid of topological derivative-based level set method and isogeometric analysis for structural topology optimization”, *Steel Compos. Struct.*, **Int. J.**, **21**(6), 1389-1410. <http://dx.doi.org/10.12989/scs.2016.21.6.1389>
- Scarpa, F., Adhikari, S. and Phani, A.S. (2009), “Effective elastic mechanical properties of single layer graphene sheets”, *Nanotechnology*, **20**, Art No. 065709. <https://doi.org/10.1088/0957-4484/20/6/065709>
- Shen, H.S. and Xiang, Y. (2018a), “Postbuckling behavior of functionally graded graphene-reinforced composite laminated cylindrical shells under axial compression in thermal environments”, *Comput. Methods Appl. Mech. Eng.*, **330**, 64-82. <https://doi.org/10.1016/j.cma.2017.10.022>
- Shen, H.S. and Xiang, Y. (2018b), “Postbuckling of functionally graded graphene-reinforced composite laminated cylindrical shells subjected to external pressure in thermal environments”, *Thin-Wall. Struct.*, **124**, 151-160. <https://doi.org/10.1016/j.tws.2017.12.005>
- Shen, H.S., Xiang, Y. and Lin, F. (2017a), “Nonlinear bending and thermal postbuckling of functionally graded graphene-reinforced composite laminated beams resting on elastic foundations”, *Eng. Struct.*, **140**, 89-97. <https://doi.org/10.1016/j.engstruct.2017.02.069>
- Shen, H.S., Xiang, Y., Lin, F. and Hui, D. (2017b), “Buckling and postbuckling of functionally graded graphene-reinforced composite laminated plates in thermal environments”, *Compos. Part B: Eng.*, **119**, 67-78. <https://doi.org/10.1016/j.compositesb.2017.03.020>
- Shen, H.S., Xiang, Y. and Lin, F. (2017c), “Thermal buckling and postbuckling of functionally graded graphene-reinforced composite laminated plates resting on elastic foundations”, *Thin-Wall. Struct.*, **118**, 229-237. https://doi.org/10.1016/j.tws.2017.05.006_
- Shen, H.S., Xiang, Y. and Lin, F. (2018), “Postbuckling of functionally graded graphene-reinforced composite laminated cylindrical panels under axial compression in thermal environments”, *Int. J. Mech. Sci.*, **135**, 398-409. <https://doi.org/10.1016/j.ijmecsci.2017.11.031>
- Song, M., Yang, J., Kitipornchai, S. and Zhu, W. (2017), “Buckling and postbuckling of biaxially compressed functionally graded multilayer graphene nanoplatelet-reinforced polymer composite plates”, *Int. J. Mech. Sci.*, **131**, 345-355. <https://doi.org/10.1016/j.ijmecsci.2017.07.017>
- Song, M., Yang, J. and Kitipornchai, S. (2018), “Bending and buckling analyses of functionally graded polymer composite plates reinforced with graphene nanoplatelets”, *Compos. Part B: Eng.*, **134**, 106-113. <https://doi.org/10.1016/j.compositesb.2017.09.043>
- Stankovich, S., Dikin, D.A., Dommett, G.H.B., Kohlhaas, K.M. Zimney, E.J., Stach, E.A., Piner, E.D., Nguyen, S.T. and Ruoff, R.S. (2006), “Graphene-based composite materials”, *Nature*, **442**, 282-286. <https://doi.org/10.1038/nature04969>
- Thanh, N.V., Khoa, N.D., Tuan, N.D., Tran, P. and Duc, N.D. (2016), “Nonlinear dynamic response and vibration of functionally graded carbon nanotube-reinforced composite (FG-CNTRC) shear deformable plates with temperature-dependent material”, *J. Thermal Stress.*, **40**, 1254-1274. <https://doi.org/10.1080/01495739.2017.1338928>
- Thom, D.V., Kien, N.D., Duc, N.D., Duc, D.H. and Tinh, B.Q. (2017), “Analysis of bi-directional functionally graded plates by FEM and a new third-order shear deformation plate theory”, *Thin-Wall. Struct.*, **119**, 687-699. <https://doi.org/10.1016/j.tws.2017.07.022>
- Vuong, P.M. and Duc, N.D. (2018), “Nonlinear response and buckling analysis of eccentrically stiffened FGM toroidal shell segments in thermal environment”, *Aerosp. Sci. Technol.*, **79**, 383-398. <https://doi.org/10.1016/j.ast.2018.05.058>
- Wang, Y., Feng, C., Zhao, Z. and Yang, J. (2018a), “Buckling of graphene platelet reinforced composite cylindrical shell with cutout”, *Int. J. Struct. Stab. Dyn.*, **18**, Article Number 1850040. <https://doi.org/10.1142/S0219455418500402>
- Wang, Y., Feng, C., Zhao, Z., Lu, F. and Yang, J. (2018b), “Torsional buckling of graphene platelets (GPLs) reinforced functionally graded cylindrical shell with cutout”, *Compos. Struct.*, **197**, 72-97. <https://doi.org/10.1016/j.compstruct.2018.05.056>
- Wang, Y., Feng, C., Zhao, Z. and Yang, J. (2018c), “Eigenvalue buckling of functionally graded cylindrical shells reinforced with graphene platelets (GPL)”, *Compos. Struct.*, **202**, 38-46. <https://doi.org/10.1016/j.compstruct.2017.10.005>
- Wu, H., Kitipornchai, S. and Yang, J. (2017), “Thermal buckling and postbuckling of functionally graded graphene nanocomposite plates”, *Mater. Des.*, **132**, 430-441. <https://doi.org/10.1016/j.matdes.2017.07.025>
- Yang, J., Wu, H. and Kitipornchai, S. (2017), “Buckling and postbuckling of functionally graded multilayer graphene platelet-reinforced composite beams”, *Compos. Struct.*, **161**, 111-118. <https://doi.org/10.1016/j.compstruct.2016.11.048>
- Yang, J., Chen, D. and Kitipornchai, S. (2018a), “Buckling and free vibration analyses of functionally graded graphene reinforced porous nanocomposite plates based on Chebyshev-Ritz method”, *Compos. Struct.*, **193**, 281-294. <https://doi.org/10.1016/j.compstruct.2018.03.090>
- Yang, Z., Yang, J., Liu, A. and Fu, J. (2018b), “Nonlinear in-plane instability of functionally graded multilayer graphene reinforced composite shallow arches”, *Compos. Struct.*, **204**, 301-312. <https://doi.org/10.1016/j.compstruct.2018.07.072>
- Yu, Y., Shen, H.S., Wang, H. and Hui, D. (2018), “Postbuckling of sandwich plates with graphene-reinforced composite face sheets in thermal environments”, *Compos. Part B: Eng.*, **135**, pp. 72-83.

<https://doi.org/10.1016/j.compositesb.2017.09.045>

Zhang, Y.Y., Wang, C.M., Cheng, Y. and Xiang, Y. (2011), "Mechanical properties of bilayer graphene sheets coupled by sp³ bonding", *Carbon*, **49**, 4511-4517.

<https://doi.org/10.1016/j.carbon.2011.06.058>

Zhao, X., Zhang, Q., Chen, D. and Lu, P. (2010), "Enhanced mechanical properties of graphenebased poly(vinyl alcohol) composites", *Macromolecules*, **43**, 2357-2363.

<https://doi.org/10.1021/ma902862u>

CC